Application of Bayesian Inference to Milling Force Modeling

Jaydeep M. Karandikar
Department of Mechanical Engineering and Engineering Science, University of North Carolina at Charlotte, Charlotte, NC 28223

Tony L. Schmitz
Department of Mechanical Engineering and Engineering Science, University of North Carolina at Charlotte, Charlotte, NC 28223

Ali E. Abbas
Department of Industrial and Enterprise Systems Engineering, University of Illinois at Urbana-Champaign, Urbana, IL 61801

This paper describes the application of Bayesian inference to the identification of force coefficients in milling. Mechanistic cutting force coefficients have been traditionally determined by performing a linear regression to the mean force values measured over a range of feed per tooth values. This linear regression method, however, yields a deterministic result for each coefficient and requires testing at several feed per tooth values to obtain a high level of confidence in the regression analysis. Bayesian inference, on the other hand, provides a systematic and formal way of updating beliefs when new information is available while incorporating uncertainty. In this work, mean force data is used to update the prior probability distributions (initial beliefs) of force coefficients using the Metropolis-Hastings (MH) algorithm Markov chain Monte Carlo (MCMC) approach. Experiments are performed at different radial depths of cut to determine the corresponding force coefficients using both methods and the results are compared. [DOI: 10.1115/1.4026365]

Keywords: milling, force, probabilistic, Bayesian inference, Markov chain Monte Carlo, uncertainty

1 Introduction

In metal cutting operations, the cutting force can be modeled using the chip area and empirical constants that depend on the tool-workpiece combination. The mechanistic cutting force coefficients are determined using a linear regression to the mean force values measured over a range of feed per tooth values [1]. However, the least squares method has two limitations. First, the method required testing at several feed per tooth values to achieve a high level of confidence in the regression. Second, for micromilling applications or machining parameters (radial and axial depth) resulting in a mean force value close to zero, the signal to noise ratio is very small which can result in a poor least squares fit. To address these limitations, the paper demonstrates milling force modeling using the MCMC method for Bayesian inference. The advantage of using Bayesian inference is that experiments over multiple feed per tooth values, which can be time consuming and costly, are not necessary for determining the cutting force coefficient values. In addition, the uncertainty in the force coefficients can be evaluated by combining prior knowledge and experimental data. The main contribution of the paper is to propose Bayesian inference for milling force modeling and compare the results with the well-known linear regression approach. The remainder of the paper is organized as follows. First, generalized expressions for mechanistic cutting force coefficients are developed. Section 2 then introduces Bayes' rule. Section 3 demonstrates the MCMC algorithm for Bayesian inference using a simple example followed by the application to milling force modeling in Sec. 4. Section 5 describes the experimental results and a comparison to the linear regression approach. Section 6 discusses the benefits of Bayesian inference followed by conclusions in Sec. 7.

In milling, the tangential, F_t, and normal, F_n, direction force components can be described using Eqs. (1) and (2), where b is the chip width (axial depth of cut), h is the instantaneous chip thickness, K_t is the tangential cutting force coefficient, K_{te} is the tangential edge coefficient, K_n is the normal cutting force coefficient, and K_{ne} is the normal edge coefficient [1].

$$F_t = K_t b h + K_{te} b \tag{1}$$

$$F_n = K_n b h + K_{ne} b \tag{2}$$

The chip thickness is time-dependent in milling and can be approximated using the feed per tooth, f_t, and time-dependent cutter angle, ϕ, provided the ratio of the feed per tooth to cutter diameter is small [2]. See below equation

$$h = f_t \sin(\phi) \tag{3}$$

The forces in the x (feed) and y directions[1], F_x and F_y, are determined by projecting the tangential and normal force components in the x and y directions using the cutter angle as shown in Fig. 1. See below equations

$$F_x = K_t b f_t \sin(\phi)\cos(\phi) + K_{te} b \cos(\phi) + K_n b f_t \sin^2(\phi) + K_{ne} b \sin(\phi) \tag{4}$$

$$F_y = K_t b f_t \sin^2(\phi) + K_{te} b \sin(\phi) - K_n b f_t \sin(\phi)\cos(\phi) - K_{ne} b \cos(\phi) \tag{5}$$

Expressions for the mean forces in the x and y directions, $\bar{F}_x$ and $\bar{F}_y$, are provided in Eqs. (6) and (7), where N_t is the number of teeth on the cutter and ϕ_s and ϕ_e are the cut start and exit angles, which are defined by the radial depth of cut [1].

$$\bar{F}_x = \left[\frac{N_t b f_t}{8\pi}(-K_t \cos(2\phi) + K_n(2\phi - \sin(2\phi))) + \frac{N_t b}{2\pi}(K_{te}\sin(\phi) - K_{ne}\cos(\phi))\right]_{\phi_s}^{\phi_e} \tag{6}$$

$$\bar{F}_y = \left[\frac{N_t b f_t}{8\pi}(K_t(2\phi - \sin(2\phi)) + K_n \cos(2\phi)) - \frac{N_t b_t}{2\pi}(K_{te}\cos(\phi) + K_{ne}\sin(\phi))\right]_{\phi_s}^{\phi_e} \tag{7}$$

Contributed by the Manufacturing Engineering of ASME for publication in the Journal of Manufacturing Science and Engineering. Manuscript received July 29, 2011; final manuscript received December 19, 2013; published online January 3, 2014. Assoc. Editor: Suhas Joshi.

[1]The z direction is oriented along the tool axis.

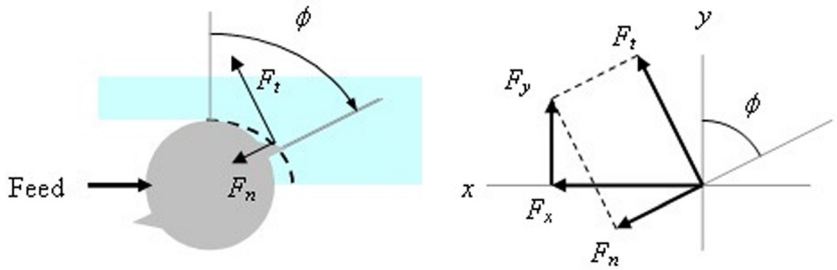

Fig. 1 Milling force geometry (a 50% radial immersion up milling cut using a cutter with two teeth is depicted)

In the Eqs. (6) and (7) average force expressions, the first term, which is a function of the feed per tooth, gives the slope of the linear regression to the average force values that correspond to the selected feed per tooth values. The second term, which does not include the feed per tooth, is the intercept of the linear regression. By rearranging Eqs. (6) and (7), the four force coefficients are determined using Eqs. (8)–(11), where $a_{1,x}$ and $a_{1,y}$ are the slopes of the linear regressions to the x and y direction average force data and $a_{0,x}$ and $a_{0,y}$ are the intercepts.

$$K_t = \frac{8\pi}{N_t b}\frac{a_{1,y}(2\phi_e - 2\phi_s + \sin(2\phi_s) - \sin(2\phi_e)) + a_{1,x}(\cos(2\phi_s) - \cos(2\phi_e))}{(2\phi_e - 2\phi_s + \sin(2\phi_s) - \sin(2\phi_e))^2 + (\cos(2\phi_e) - \cos(2\phi_s))^2} \tag{8}$$

$$K_n = \frac{8\pi}{N_t b}\frac{a_{1,y}(\cos(2\phi_e) - \cos(2\phi_s)) + a_{1,x}(2\phi_e - 2\phi_s + \sin(2\phi_s) - \sin(2\phi_e))}{(2\phi_e - 2\phi_s + \sin(2\phi_s) - \sin(2\phi_e))^2 + (\cos(2\phi_e) - \cos(2\phi_s))^2} \tag{9}$$

$$K_{te} = \frac{\pi}{N_t b}\frac{a_{0,x}(\sin(\phi_e) - \sin(\phi_s)) - a_{0,y}(\cos(\phi_e) - \cos(\phi_s))}{1 - \cos(\phi_e - \phi_s)} \tag{10}$$

$$K_{ne} = \frac{-\pi}{N_t b}\frac{a_{0,x}(\cos(\phi_e) - \cos(\phi_s)) + a_{0,y}(\sin(\phi_e) - \sin(\phi_s))}{1 - \cos(\phi_e - \phi_s)} \tag{11}$$

2 Bayesian Inference

Bayesian inference, which forms a normative and rational method for belief updating, is applied for force coefficient determination here. Bayesian inference models are used to update a user's belief about an uncertain variable when new information becomes available (e.g., an experimental result). Bayes' rule is given by

$$\{A|B,\&\} = \frac{\{A|\&\}\{B|A,\&\}}{\{B|\&\}}, \tag{12}$$

where $\{A\,|\,\&\}$ is the prior distribution about an uncertain event, A, at a state of information, &; $\{B\,|\,A,\&\}$ is the likelihood of obtaining an experimental result B given that event A has occurred; $\{B\,|\,\&\}$ is the probability of obtaining experimental result B (without knowing that A has occurred); and $\{A\,|\,B,\&\}$ is the posterior belief about event A after observing the result, B. According to Bayes' rule, the product of the prior and likelihood functions is used to determine the posterior belief. This is the process of learning, i.e., updating the prior belief given the new data B to obtain the posterior belief. Note that $\{B\,|\,\&\}$ acts as a normalizing constant when updating probability density functions (pdf).

For the case of updating the four force coefficients in Eqs. (8)–(11) using experimental force data, Bayes' rule is written as

$$f_{K_t,K_n,K_{te},K_{ne}}(K_t,K_n,K_{te},K_{ne}|\bar{F}_{x,m},\bar{F}_{y,m}) \propto f_{K_t,K_n,K_{te},K_{ne}}\, l(\bar{F}_{x,m},\bar{F}_{y,m}|K_t,K_n,K_{te},K_{ne}) \tag{13}$$

where $f_{K_t,K_n,K_{te},K_{ne}}(K_t,K_n,K_{te},K_{ne}|\bar{F}_{x,m},\bar{F}_{y,m})$ is the posterior distribution of the force coefficients given measured values[2] of the mean forces in the x and y directions, $\bar{F}_{x,m}$ and $\bar{F}_{y,m}$, $f_{K_t,K_n,K_{te},K_{ne}}$ is the prior distributions of the force coefficients, and $l(\bar{F}_{x,m},\bar{F}_{y,m}|K_t,K_n,K_{te},K_{ne})$ is the likelihood of obtaining the measured mean force values given specified values of the force coefficients. The posterior (i.e., the new belief after updating) is proportional to the prior multiplied by the likelihood. For multiple measurements, Bayes' rule can incorporate all data in a single calculation. The likelihood functions for each measurement are multiplied together to obtain a total likelihood function. The posterior pdf is calculated by multiplying the prior and the total likelihood function. Note that the posterior distributions must be normalized so that a unit volume under the pdf is obtained; this is the purpose of the denominator in Eq. (12).

[2]The subscript m denotes measured values from cutting experiments. The measured values were assumed to be statistically independent in this study.

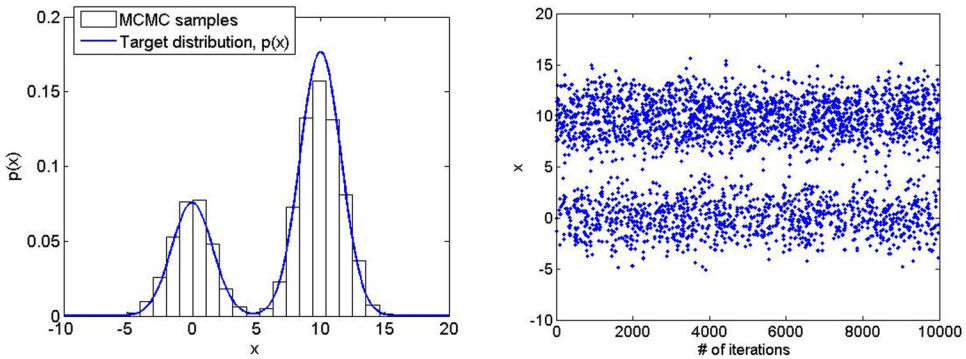

Fig. 2 Histogram of MCMC samples and target distribution (left) and *x* values for each iteration (right)

3 Markov Chain Monte Carlo (MCMC) method

The MCMC method is a strategy used to draw samples, x^i, from a random (known) distribution, x, where i is the sample (or iteration) number. The distribution of interest is referred to as a target distribution and is denoted as $p(x)$. Using the MCMC method, samples are generated from the state space, X, using a Markov chain mechanism [3]. The MH algorithm is the most widely used MCMC method [4,5]. In the MH algorithm, a candidate sample, x^* is drawn from a proposal distribution, $q(x)$. It is selected given the current value of x according to $q(x^* \mid x^i)$. The candidate sample is either accepted or rejected depending on an acceptance ratio, A. At each iteration, the Markov chain moves to x^* if the sample is accepted. Otherwise, the chain remains at the current value of x. The MH algorithm is completed over $N-1$ iterations as follows.

(1) Initialize the starting point x^0.
(2) For $i=0$ to $i=N-1$ iterations, complete the following four steps:
(a) randomly sample x^* from the proposal pdf $q(x^* \mid x^i)$
(b) randomly sample u from a uniform distribution of values between 0 and 1, $U(0, 1)$
(c) compute the acceptance ratio, $A = \min\left(1, \frac{p(x^*)q(x^i \mid x^*)}{p(x^i)q(x^* \mid x^i)}\right)$
(d) if $u < A$, then set the new value equal to the new sample, $x^{i+1} = x^*$; otherwise, the value remains unchanged $x^{i+1} = x^i$.

Table 1 Time-domain simulation parameters

Parameter	Value
Tool diameter (mm)	19.05
Radial depth (mm)	4.76
Axial depth (mm)	3.0
Spindle speed (rpm)	5000
Feed per tooth (mm/tooth)	0.03, 0.04, 0.05, 0.06, 0.07
Number of teeth	1
Helix angle (deg)	0
Tangential coefficient (N/mm^2)	2200
Normal coefficient (N/mm^2)	1200
Tangential edge coefficient (N/mm)	50
Normal edge coefficient (N/mm)	50

Table 2 Mean force values obtained from the time-domain simulation

f_t (mm/tooth)	$\bar{F}_{x,m}$ (N)	$\bar{F}_{y,m}$ (N)
0.03	−15.40	49.01
0.04	−17.58	54.40
0.05	−19.76	59.80
0.06	−21.94	65.19
0.07	−24.12	70.59

3.1 Algorithm Demonstration. To illustrate the algorithm, consider a target pdf described by the bimodal pdf in Eq. (14) [3]. Note that the normalization constant of the target pdf does not need to be known.

$$p(x) \propto 0.3e^{(-0.2x^2)} + 0.7e^{(-0.2(x-10)^2)} \tag{14}$$

For this example, a normal proposal distribution, $q(x)$, was chosen with a mean of x^i and a standard deviation of 10, i.e., $q(x) = N(x^i, 10)$. The starting point of the chain, x^0, was selected to be zero. At each iteration, i, the following steps were completed. First, a candidate sample, x^*, was randomly drawn from $N(x^i, 10)$. The candidate sample was drawn given the current value of the chain, $q(x^* \mid x^i)$. In other words, the proposal distribution is conditioned on the current value of the chain. To illustrate, consider the first iteration. The chain starting point is $x^0 = 0$. Therefore, x^* is a random sample drawn from $N(0, 10)$. Assume the randomly selected value is $x^* = 2$ and it is accepted as x^1. In the second iteration, the random sample is drawn from $N(2, 10)$. If the sample is 12 and it is rejected, then the current value of x^2 remains at 2. In the third iteration, the random sample will again be drawn from $N(2, 10)$.[3]

In the second step, $p(x^*)$ and $p(x^i)$ were calculated using Eq. (14) for the target distribution. Third, $q(x^* \mid x^i)$ and $q(x^i \mid x^*)$ were calculated, where $q(x^* \mid x^i)$ was the pdf value of the normal proposal distribution at x^* given a mean equal to x^i and a standard deviation of 10. Similarly, $q(x^i \mid x^*)$ was the pdf value of the normal proposal distribution at x^i given a mean of x^* with a standard deviation of 10. Fourth, the acceptance ratio, A, was calculated. Because normal distributions were used, the equality $q(x^* \mid x^i) = q(x^i \mid x^*)$ holds and the acceptance ratio simplified to

$$A = \min\left(1, \frac{p(x^*)}{p(x^i)}\right) \tag{15}$$

Fifth, A was compared to a random sample, u, drawn from a uniform distribution with a range from 0 to 1. Finally, if u was less than A, then the candidate sample was accepted so that $x^{i+1} = x^*$. Otherwise, it was rejected and $x^{i+1} = x^i$. These steps were repeated for $N-1$ iterations to obtain N samples of x from the target pdf described by Eq. (14).

[3]If the proposal distribution was chosen to be uniform, then it is not dependent on the current value of x. In that case, x^* will be drawn from $U(x_{\min}, x_{\max})$, where $x_{\min}$ is the minimum value and $x_{\max}$ is the maximum value of x for the uniform proposal distribution. A uniform proposal distribution is therefore less efficient because the random samples are independent of the current state of the chain. The random samples have an equal probability of taking any value between $x_{\min}$ and $x_{\max}$ which leads to many rejections. Using a normal proposal distribution, where x^* is dependent on x^i is referred to as random walk Metropolis sampling, while the uniform proposal approach where x^* is independent of x^i is called independent Metropolis Hastings sampling.

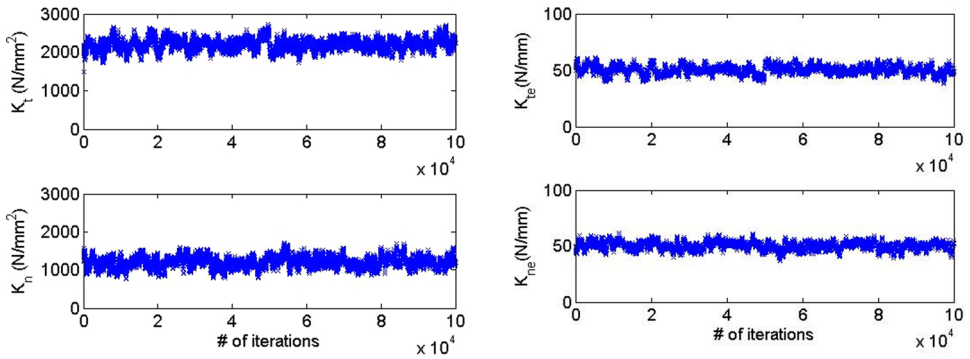

Fig. 3 Traces of K_t and K_n (left) and K_{te} and K_{ne} (right)

The MH algorithm was carried out for 1×10^4 iterations. Figure 2 shows the histogram of the 10,000 samples and target distribution from Eq. 14 (left) and x values for each iteration (right). It is observed that the samples approximate the target pdf quite well. Note that the histogram and target distribution were normalized to obtain a unit area.

Although the MH algorithm is effective for sampling from any target distribution, there are a number of considerations in its application. The success of the algorithm depends on the choice of proposal distribution. In theory, the chain should converge to the stationary target distribution for any proposal distribution [6]. However, the proposal distribution may affect the convergence and mixing of the chain. In general, the proposal distribution may be selected so that the sampling is convenient. For a normal proposal distribution (that was chosen in this example), the choice of the standard deviation can also affect the results. A larger standard deviation causes greater jumps around the current value. Thus, the candidate sample has a higher probability of being rejected, which yields $x^{i+1} = x^i$. On the other hand, while a smaller variance will tend to accept a higher number of random samples, it results in slower convergence of the chain.

In practice, the initial iterations are typically discarded and the chain subsequently settles to a stationary distribution. This is referred to as the burn-in time of the chain. A practical way to evaluate convergence to the chain's stationary distribution is by observing the traces and histograms of the variables (e.g., see Fig. 2). The number of iterations should be large enough to ensure convergence to the statistical moments of the target distribution. The starting value of the chain has no effect for a large number of iterations [6–8]. The convergence to the true statistical moments can be observed by repeating the algorithm using different starting values and varying the number of iterations. Despite these potential limitations, the MH algorithm (for MCMC) works well and can effectively be used to draw samples from multivariate distributions.

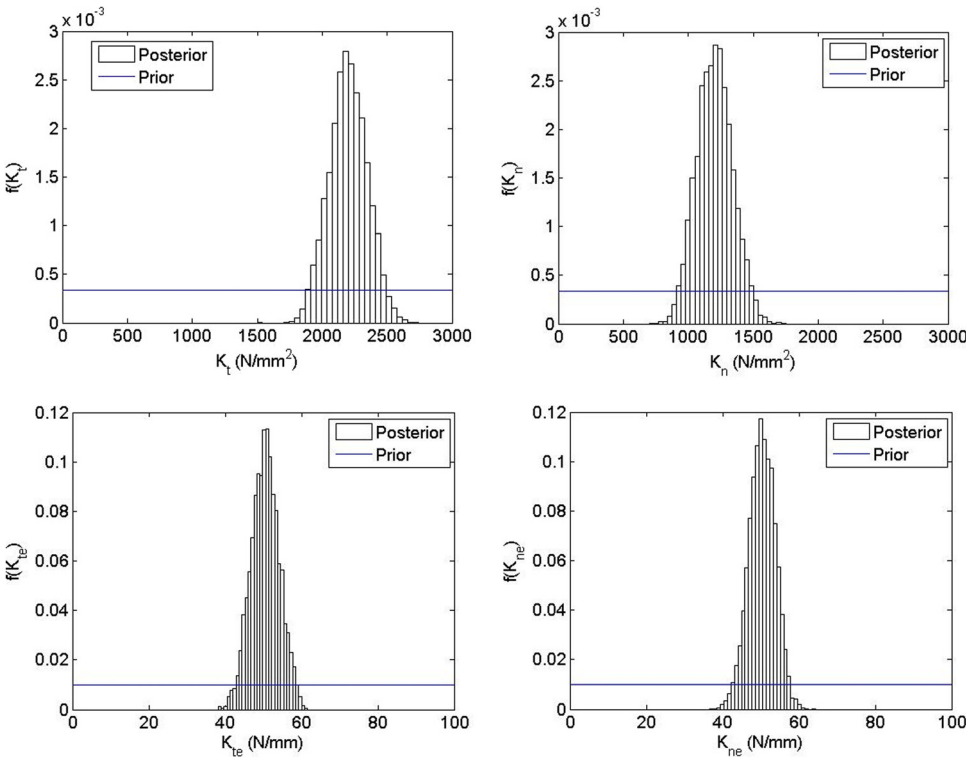

Fig. 4 Posterior and prior distributions of K_t (top left), K_n (top right), K_{te} (bottom left), and K_{ne} (bottom right) using a uniform prior. Note that the area under the histogram was normalized to unity in each case.

Table 3 Comparison of the force coefficient distributions from MCMC to the true values using a uniform prior

	True value	μ	% error	σ
K_t (N/mm^2)	2200	2201.2	0.05	136.9
K_n (N/mm^2)	1200	1207.2	0.6	139.6
K_{te} (N/mm)	50	50.7	1.2	3.51
K_{ne} (N/mm)	50	49.8	−0.6	3.43

Table 4 Correlation coefficients between the force coefficients

	K_t	K_n	K_{te}	K_{ne}
K_t	1.00	−0.11	−0.95	−0.05
K_n	−0.11	1.00	0.26	−0.95
K_{te}	−0.95	0.26	1.00	−0.11
K_{ne}	−0.05	−0.95	−0.11	1.00

Table 5 Posterior force coefficient distributions with varying uncertainty in the force data. The standard deviations are emphasized using a bold font.

	Force uncertainty, 1σ		
	0.5 N	1 N	2 N
K_t	N(2192.2, **75.7**)	N(2201.2, **136.9**)	N(2211.2, **254.0**)
K_n	N(1201.2, **67.5**)	N(1207.2, **139.9**)	N(1197.2, **252.0**)
K_{te}	N(50.8, **1.9**)	N(50.7, **3.5**)	N(49.7, **6.4**)
K_{ne}	N(49.8, **1.7**)	N(49.8, **3.4**)	N(50.5, **6.3**)

3.2 Application to Bayesian Inference. This section describes the application of MCMC to Bayesian inference. As stated in Sec. 2, Bayesian inference provides a formal way to update beliefs about the posterior distribution (the normalized product of the prior and the likelihood functions) using experimental results. In the case of updating force coefficients (Eq. (13)), the prior is a joint pdf of the force coefficients, K_t, K_n, K_{te}, and K_{ne}. As a result, the posterior is also a joint pdf of the force coefficients. In Bayesian inference, the MCMC technique can be used to sample from multivariate posterior distributions. The single-component MH algorithm facilitates sampling from multivariate distributions without sensitivity to the number of variables [7]. The joint posterior pdf is the target pdf for MCMC. The posterior, or target, pdf is the product of the prior and likelihood density functions. Note that the normalizing constant of the posterior pdf is not required for sampling.

The MH algorithm was detailed for a single variable in Sec. 3. To sample from a joint pdf, the algorithm samples one variable at a time and then proceeds sequentially to sample the remaining variables. The sequence of variable sampling does not influence the convergence of the algorithm. To illustrate, consider a joint target pdf of n variables: $x_1, x_2, x_3, \ldots, x_n$. To begin, the starting value for all the variables is initialized, $[x_1^0, x_2^0, x_3^0, \ldots, x_n^0]$. Let the algorithm proceed in the order, $x_1 \rightarrow x_2 \rightarrow x_3 \rightarrow \ldots x_n$. The sampling for each variable is carried out using a univariate proposal distribution for that variable. The proposal distribution for each variable can be different or the same. Since the algorithm proceeds one variable at a time, the target and the proposal pdf for each variable is conditioned on the current values of the other variables. For example, consider a candidate sample, x_1^*, drawn from the univariate proposal distribution for x_1. The candidate sample from the joint pdf is then $[x_1^*, x_2^0, x_3^0, \ldots, x_n^0]$. The candidate sample, x_1^*, is either accepted or rejected given the current values of $x_2, x_3, \ldots, x_n$. Thus, the target pdf values of x_1^* and x_1^0 are conditional on the current values of the other variables, $x_2^0, x_3^0, \ldots, x_n^0$ and are denoted as $p(x_1^* \mid x_1^0, x_2^0, \ldots, x_n{}^0)$ and $p(x_1^0 \mid x_1^0, x_2^0, \ldots, x_n^0)$. The proposal univariate pdfs are also conditional on the current values of the chain and are denoted as $q(x_1{}^* \mid x_1, x_2, x_3, \ldots, x_n)$ and $q(x_1 \mid x_1{}^*, x_1, x_3, \ldots, x_n)$ for $x_1{}^*$ and x_1, respectively. To summarize, the chain either stays at the current point, $[x_1^0, x_2^0, x_3^0, \ldots, x_n^0]$ or moves to a neighboring point, $[x_1^*, x_2^0, x_3^0, \ldots, x_n^0]$, which differs only in one component of the current state (x_1 in this case). The procedure is repeated for all variables in each iteration. The acceptance ratio is

$$A = \min\left(1, \frac{p(x_1^*|x_2, x_3 \ldots x_n) q(x_1^i | [x_1^*, x_2, x_3 \ldots x_n])}{p(x_1^i|x_2, x_3 \ldots x_n) q(x_1^* | [x_1^i, x_2, x_3 \ldots x_n])}\right) \tag{16}$$

where the value of each of the four joint pdfs must each be calculated. The value of A is compared to a random sample, u, from a uniform distribution with a range from 0 to 1 and x_1^* is either accepted or rejected to obtain $x_1{}^{i+1}$. The algorithm is repeated using the updated values of each variable continually for the next variable. Thus, $x_2{}^{i+1}$ is determined using $x_1{}^{i+1}, x_3{}^i, \ldots, x_n{}^i$, $x_3{}^{i+1}$ is determined using $x_1{}^{i+1}, x_2{}^{i+1}, \ldots x_n{}^i$, and so on for n variables. The algorithm therefore moves by a small step in the joint pdf by sampling a single variable at a time. A single iteration updates all the variables. The algorithm is then carried out for N iterations to obtain samples from the joint target pdf. An alternative method is to sample from a joint proposal pdf and accept or reject it using the MH algorithm. However, it is much simpler to sample from univariate proposal distributions for each variable and is computationally less expensive.

4 Bayesian Updating Using the Markov Chain Monte Carlo method

In this section, the MCMC method for Bayesian updating of force coefficients is demonstrated using a numerical example. The effects of the prior and likelihood uncertainties are also evaluated. A milling time-domain simulation [1] was used to obtain the x and y directions mean force values. The tool-material combination was assumed to be a coated carbide tool and 1018 steel. The objective of the simulation was to validate the MCMC method by

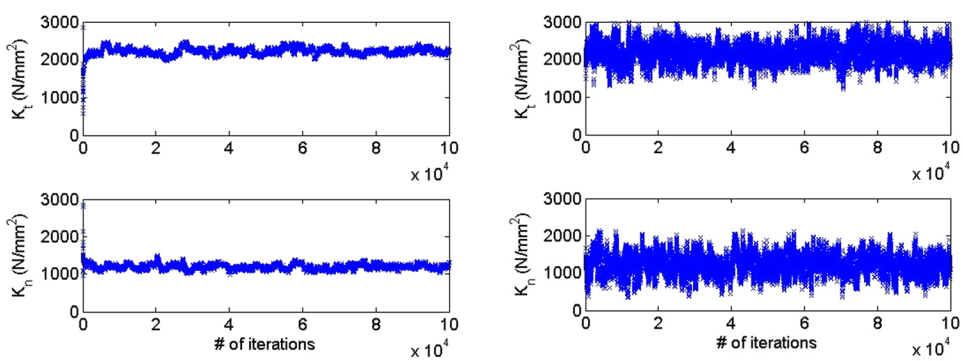

Fig. 5 Traces of K_t and K_n with 0.5 N force measurement uncertainty (left) and 2 N (right)

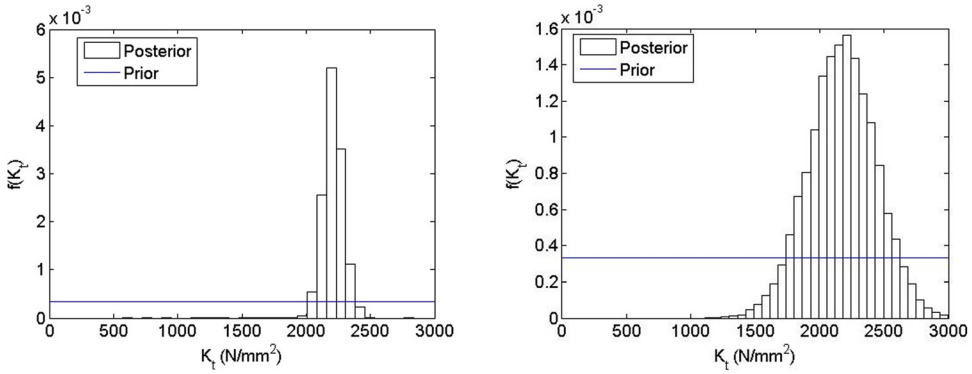

Fig. 6 Posterior and prior distributions of K_t with a force uncertainty of $\sigma = 0.5$ N (left) and $\sigma = 2$ N (right)

Table 6 Comparison of the force coefficient distributions from MCMC to the true values using a normal prior

	True value	μ	% error	σ
K_t (N/mm^2)	2200	2240.2	1.8	224.6
K_n (N/mm^2)	1200	1059.6	−8.8	243.7
K_{te} (N/mm)	50	50.2	0.4	5.58
K_{ne} (N/mm)	50	55.6	11.2	7.17

comparing its solution to the known force coefficients used to define the "measured" data via the simulation. The parameters used in the down milling simulation are listed in Table 1. The simulation was exercised at different feed per tooth values and the mean forces were recorded; see Table 2. The mean values listed in Table 2 were treated as experimental results and used to update the force coefficients' prior distributions using the MCMC method for Bayesian inference.

As described in Sec. 3.2, a single-component MH algorithm was used to sample from the joint posterior pdf of the force coefficients, K_t, K_n, K_{te}, and K_{ne}. The posterior joint pdf was the target pdf for the MH algorithm. For this analysis, the prior distribution of force coefficients was assumed to be a joint uniform distribution, i.e., it was equally likely to obtain any value within the specified range. The force coefficients were assumed to be independent for the prior. The marginal prior pdfs[4] of the force coefficients were specified as: K_t (N/mm^2) $= U(0, 3000)$, K_n (N/mm^2) $= U(0, 3000)$, K_{te} (N/mm) $= U(0, 100)$, and K_{ne} (N/mm) $= U(0, 100)$, where U represents a uniform distribution and the parenthetical terms indicated the lower and upper values of the range. As noted in Sec 3.1, this distribution represents a less informative prior than a normal distribution with a mean and standard deviation. The effect of different types of priors on the posterior distributions is discussed in Sec. 4.3.

The single-component MH algorithm proceeds as follows. First, the starting point for the Markov chain, $x^0 = \begin{bmatrix} K_t^0 & K_n^0 & K_{te}^0 & K_{ne}^0 \end{bmatrix}$, was selected to be the midpoints of the uniform K_t, K_n, K_{te}, and K_{ne} distributions, $x^0 = [\,1500 \quad 1500 \quad 25 \quad 25\,]$. The sampling was completed one coefficient at a time in the order $K_t \rightarrow K_n \rightarrow K_{te} \rightarrow K_{ne}$. A candidate sample, K_t^*, was drawn from the proposal distribution of K_t. The proposal distribution for each coefficient was selected to be normal. The posterior, or target, pdf values, of each force coefficient were conditional on the values of the other coefficients. The posterior pdf for K_t, denoted as $p(K_t^0 \,|\, K_n^0\ K_{te}^0\ K_{ne}^0)$, was the product of the prior and likelihood functions. The prior value for any coefficient was determined from the marginal prior distributions of each coefficient, which were selected to be uniform. The mean force values were calculated using the current state of the chain, $[K_t^0\ K_n^0\ K_{te}^0 K_{ne}^0]$, together with Eqs. (6) and (7) for the specified cut geometry. Because there is inherent uncertainty in milling forces, the mean force values calculated using the current state of chain and Eqs. (6) and (7) were assumed to be normally distributed with a standard deviation of 1 N, which was based on the user's belief regarding experimental uncertainty in measured force values (this value could also be specified as a percent of the nominal value, for example). The effect of the standard deviation on the posterior pdf is discussed in Sec. 4.2. This gave a pdf for both the x and y directions mean forces calculated using the current state of the chain. The likelihood for the x and y directions was the value of each pdf for the experimental mean forces (from the time-domain simulation). Therefore, the likelihood described how likely it was to obtain the experimental mean forces given the current state of the chain. For multiple measurement results, the total likelihood pdf was the product of the likelihood pdfs for all measurements. The same procedure was followed to determine the posterior pdf value for K_t^*, $p(K_t^* \,|\, K_n^i\ K_{te}^i\ K_{ne}^i)$. Since the proposal distribution was normal, the acceptance ratio was calculated using below equation.

$$A = \min\left(1, \frac{p(K_t^* | K_n, K_{te}, K_{ne})}{p(K_t^i | K_n, K_{te}, K_{ne})}\right) \tag{17}$$

The acceptance ratio was compared with a random sample, u, from a uniform distribution (with a range from 0 to 1) to assign the value of K_t^1 to be either K_t^* or K_t^0. To update the four force coefficients, K_t, K_n, K_{te}, and K_{ne}, the algorithm considered one coefficient at a time and then proceeded to sequentially update the remaining coefficients. The updated values for each coefficient were used continually for updating the next coefficient. For the order $K_t \rightarrow K_n \rightarrow K_{te} \rightarrow K_{ne}$, K_t^1 was used to update K_n^0. Next, K_t^1 and K_n^1 were used for K_{te}^0. Finally, K_t^1, K_n^1, and K_{te}^1 were used for K_{ne}^0. A single iteration provided samples for all the force coefficients. This sequence was repeated for $N-1$ iterations giving N samples from the joint posterior pdf of the coefficients. Note that the standard deviations of the proposal distributions affect the convergence of the chain. The standard deviations of the force coefficients, K_t, K_n, K_{te}, and K_{ne} were 600 N/mm^2, 600 N/mm^2, 33 N/mm, and 33 N/mm, respectively. As a rule of thumb, the standard deviation should be large enough to draw adequate samples to explore the domain. However, a very large standard deviation leads to a higher probability of candidate samples being rejected.

4.1 Results. The MH algorithm was exercised for 1×10^5 iterations. Figure 3 shows the sample traces of the force coefficients for all iterations. It is seen that there is a rapid convergence to the true values for all coefficients. The initial burn-in time was selected as 1×10^3 iterations. Figure 4 shows a comparison

[4]A marginal pdf for any variable in a joint distribution is obtained by integrating the remaining variables over all values.

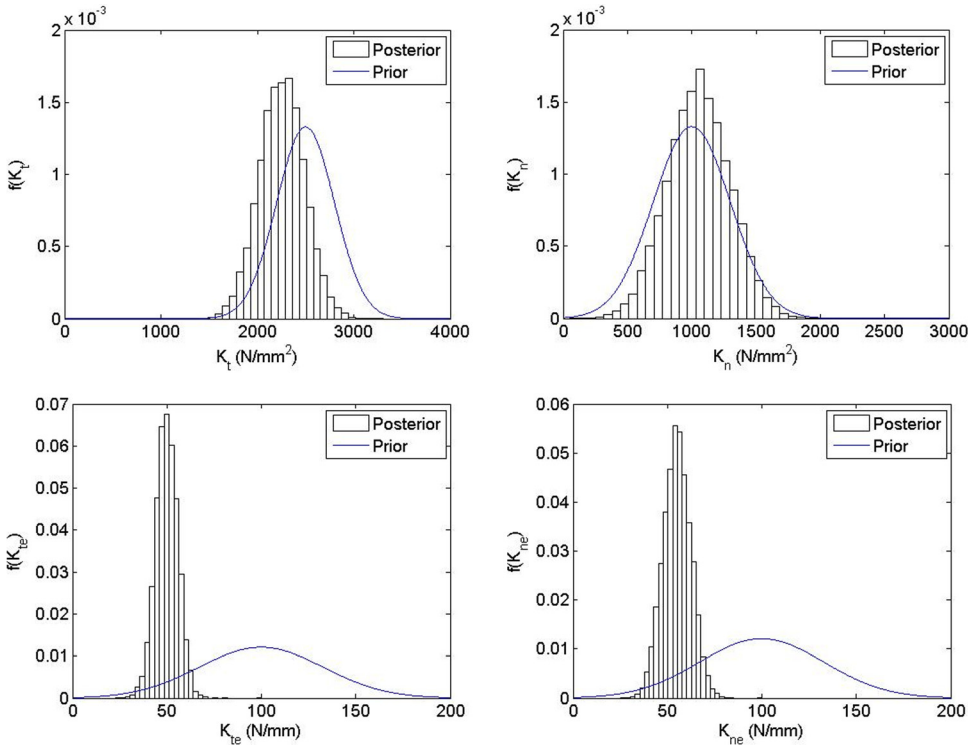

Fig. 7 Posterior and prior distributions of K_t (top left), K_n (top right), K_{te} (bottom left), and K_{ne} (bottom right) using a normal prior

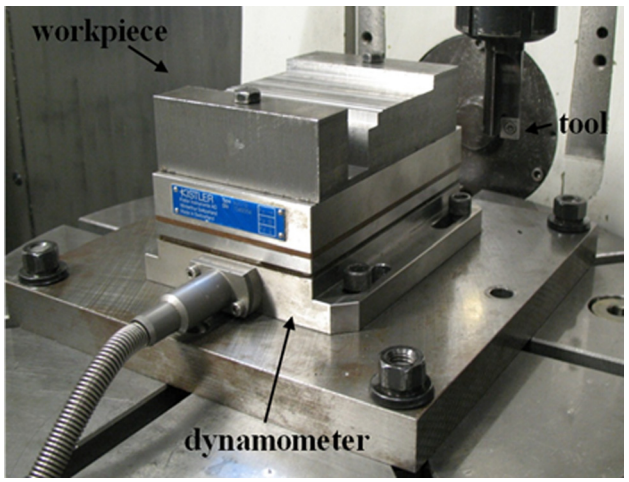

Fig. 8 Experimental setup for milling force measurement

Table 7 Experimental mean forces in *x* and *y* directions and force coefficients obtained using linear regression at 25% radial immersion

f_t (mm/tooth)	Mean F_x (N)	Mean F_y (N)	K_t (N/mm^2)	K_n (N/mm^2)	K_{te} (N/mm)	K_{ne} (N/mm)
0.03	−11.50	40.13	2149.0	1290.1	34.7	37.1
0.04	−13.31	46.10				
0.05	−14.83	50.03				
0.06	−17.64	56.63				
0.07	−19.10	62.06				

between the prior marginal pdfs and posterior sample histograms of the force coefficients. The histograms represent the marginal posterior pdfs of the force coefficients and were normalized to obtain a unit area. The distributions in the force coefficients are due to the uncertainty in the mean force values. MCMC gives

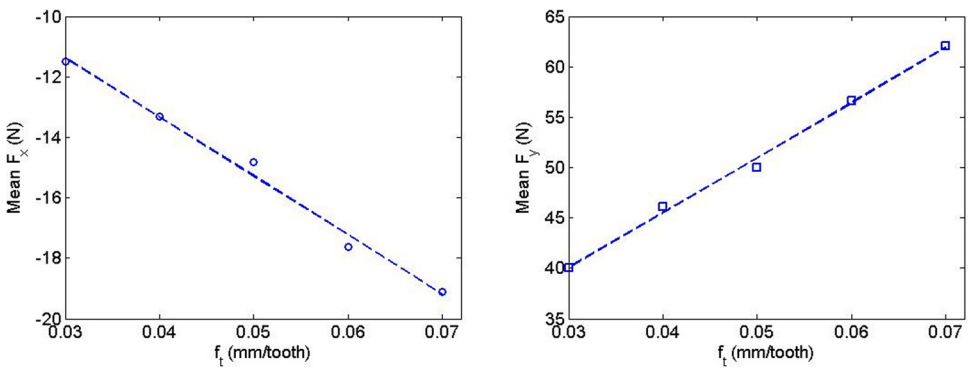

Fig. 9 Linear regression to the mean forces in *x* (left) and *y* (right) direction to determine the force coefficients at 25% radial immersion

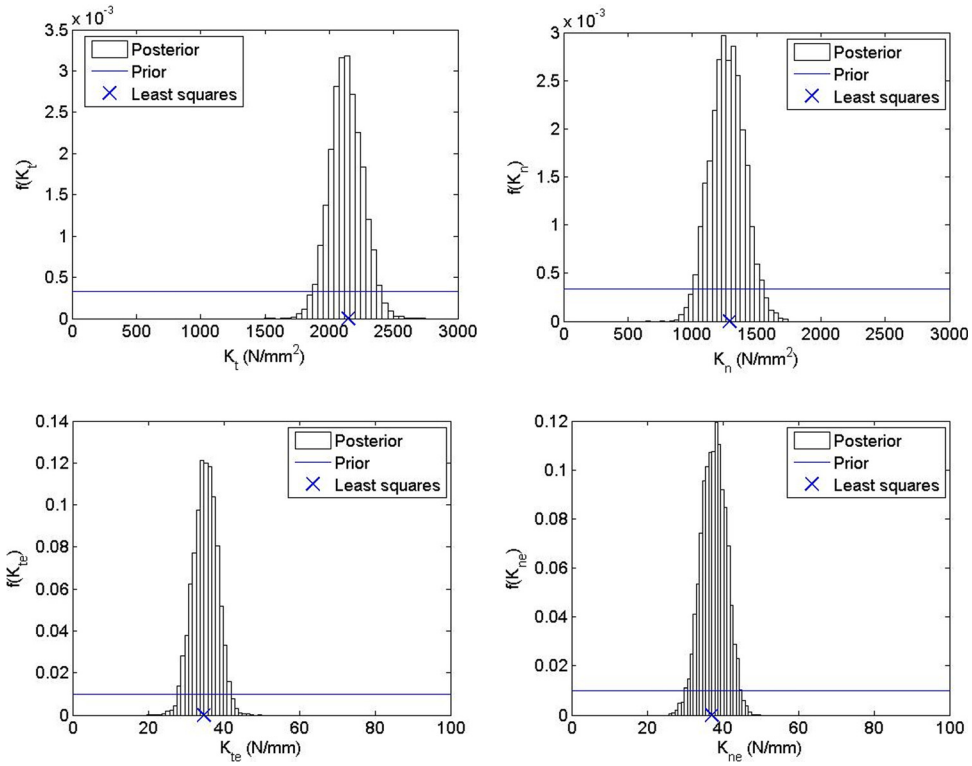

Fig. 10 Posterior and prior distributions of K_t (top left), K_n (top right), K_{te} (bottom left), and K_{ne} (bottom right). The least squares values are identified by the "x" symbols.

samples from the joint posterior pdf of the force coefficients, K_t, K_n, K_{te}, and K_{ne}. Since the prior was assumed to be a uniform distribution and the likelihood was normal, the posterior joint distribution was also a joint normal distribution. The mean, μ, and standard deviation, σ, values for the four force coefficient posterior marginal pdfs are listed in Table 3; the coefficient mean values show good agreement with the true values. Note that the coefficient distributions are not independent; the correlation coefficients between the force coefficients are listed in Table 4. Although the convergence to the true values as a function of number of iterations can be evaluated, 1×10^5 samples was found to be adequate to ensure convergence for this study. Table 4 shows that the cutting force coefficients, K_t and K_n, as well as the edge coefficients, K_{te} and K_{ne}, have a small correlation between them. However, the cutting force coefficients have a strong negative correlation with the respective edge coefficients (-0.95). The standard deviation of the posterior distributions of the force coefficients is a function of the force uncertainty used to determine the likelihood (1 N was assumed). The effect of the likelihood uncertainty on the posterior distribution is discussed in Sec. 4.2.

Using Bayesian inference, uncertainty in the force data can be propagated to determine uncertainty in the force coefficients. Furthermore, because the Bayesian updating approach does not rely on a least-squares curve fit, it eliminates data collection at several feed per tooth values. MCMC is computationally inexpensive and facilitates updating of multiple variables. The posterior samples also provide information regarding the correlation between the coefficients. These samples can be used to propagate the force coefficient uncertainty to quantify the uncertainty in the milling stability boundary, for example Ref. [9].

Table 8 Correlation coefficients between the force coefficients at 25% radial immersion

	K_t	K_n	K_{te}	K_{ne}
K_t	1.00	−0.09	−0.95	−0.08
K_n	−0.09	1.00	0.23	−0.94
K_{te}	−0.95	0.23	1.00	−0.07
K_{ne}	−0.08	−0.94	−0.07	1.00

4.2 Effect of Likelihood Uncertainty. The standard deviations of the marginal force coefficient distributions listed in Table 5 are a function of the force uncertainty level used in the likelihood calculations. To study this effect, the updating procedure was repeated with mean force uncertainties of 0.5 N and 2 N. Figure 5 shows the traces of K_t and K_n with standard deviations of 0.5 N (left) and 2 N (right). Figure 6 shows the posterior and prior pdf comparisons of K_t for the 0.5 N (left) and 2 N (right) standard deviations. It is observed in these figures that the standard deviation of the posterior distribution reduces with the likelihood uncertainty. Similar results were obtained for all the force coefficients. The standard deviations of all coefficients at different force uncertainty levels are listed in Table 5. Note that the mean converges to the true values in all cases and is not affected by the likelihood uncertainty. The likelihood uncertainty may be selected by the user based on his/her level of confidence in the experimental data.

4.3 Effect of the Prior Selection. In this section, the effect of the prior on the posterior distribution of force coefficients is studied. For the numerical results presented in Sec. 4.1, a uniform prior was selected. A uniform prior represents a noninformative case, where any coefficient value with the specified range is equally likely to be correct. To evaluate the influence of the prior distribution on the posterior pdf, the algorithm was repeated using normal marginal pdfs as the prior for the force coefficients. The marginal prior pdfs were selected as:

- K_t (N/mm^2) = $N(2500, 300)$
- K_n (N/mm^2) = $N(1200, 300)$
- K_{te} (N/mm) = $N(100, 33)$
- K_{ne} (N/mm) = $N(100, 33)$.

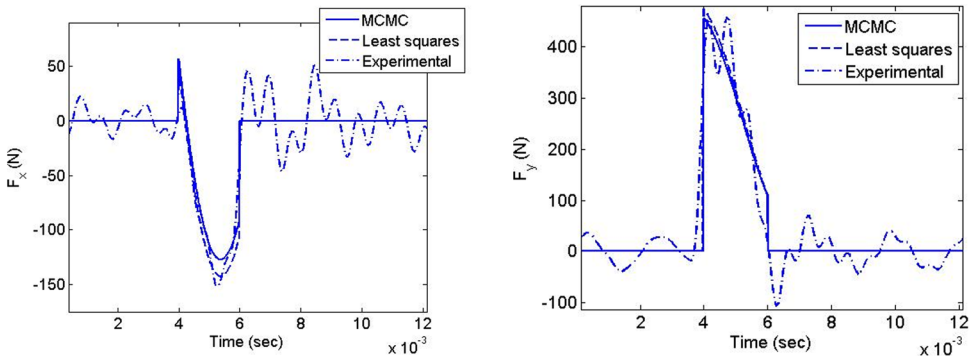

Fig. 11 Comparison of the experimental and simulated force profiles for F_x (left) and F_y (right). The simulation used the force coefficients determined using the MCMC and least squares methods. Note that the oscillations in the experimental data are due to excitation of the dynamometer dynamics by the cutting force frequency content.

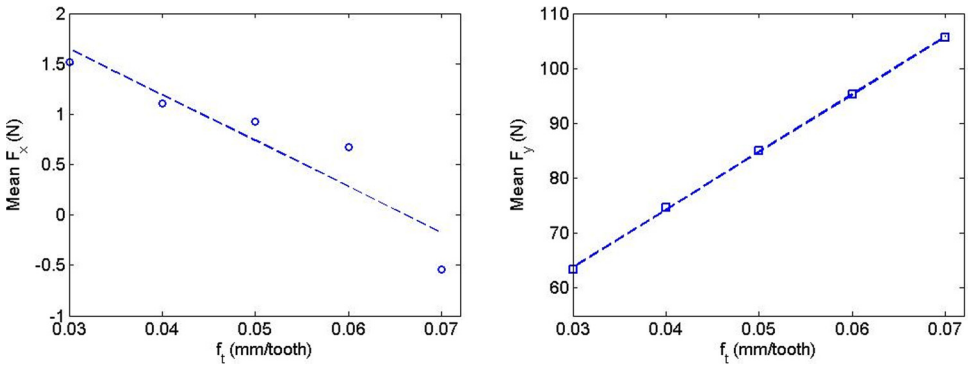

Fig. 12 Linear regression to the mean forces in the *x* (left) and *y* (right) directions used to determine the force coefficients at 50% radial immersion

Table 9 Experimental mean forces in the *x* and *y* directions and force coefficients obtained using linear regression at 50% radial immersion

f_t (mm/tooth)	Mean F_x (N)	Mean F_y (N)	K_t (N/mm^2)	K_n (N/mm^2)	K_{te} (N/mm)	K_{ne} (N/mm)
0.03	1.51	63.35	2504.6	1446.2	37.5	45.2
0.04	1.11	74.71				
0.05	0.93	84.98				
0.06	0.67	95.29				
0.07	−0.54	105.51				

Table 6 lists the mean and standard deviation for each of the four force coefficient posterior marginal pdfs. Figure 7 provides a comparison between the prior marginal pdfs and posterior sample histograms of the force coefficients. The percent errors in Table 6 (normal prior) are larger than those in Table 3 (uniform prior). The posterior distribution is clearly sensitive to the choice of the prior.

For a uniform prior, the posterior is the same as the likelihood and, therefore, the posterior mean force coefficient values converge to the true value. However, for a normal prior which includes a mean and standard deviation, the true values lie within the range of posterior distributions. Note that the posterior pdf takes into account the prior mean and the likelihood function. The prior represents the initial degree of belief about the force coefficients; if the initial belief is far from the true value, this affects the final results. The selection of the prior may be based on previous experience, values reported in the literature, or theoretical considerations. In general, the prior should be chosen to be as informative as possible considering all the available information. If enough data or prior knowledge is not available, a uniform prior may be selected. In the numerical example, the prior was chosen based on beliefs regarding the range of values the force coefficient would most likely take for the selected tool-material combination.

5 Experimental Results

This section describes the experimental setup used to perform force coefficient measurements. Cutting tests were performed with a 19 mm diameter inserted endmill (one square uncoated Kennametal 107888126 C9 JC carbide insert; zero rake and helix angles, 15 deg relief angle, 9.53 mm square × 3.18 mm). The workpiece material was 1018 steel. The cutting force was measured using a table mounted dynamometer (Kistler 9257B). Figure 8 shows the experimental setup. The first test was completed at a spindle speed, Ω, of 2500 rpm with a 3 mm axial depth of cut and 4.7 mm radial depth of cut (25% radial immersion (RI)). The force coefficients were evaluated by performing a linear regression to the mean x (feed) and y direction forces obtained over a range of feed per tooth values: $f_t = \{0.03, 0.04, 0.05, 0.06, \text{and } 0.07\}$ mm/tooth. Figure 9 shows the linear least squares best fit to the experimental mean forces in the x and y directions. The mean forces show a linear increase for both the x and y directions and the quality of fit is good ($R^2 = 0.99$). The force coefficients were determined using slopes and intercepts from the fit to the data. The values of the mean forces and the force coefficients are provided in Table 7.

The experimental force data listed in Table 7 was used to perform Bayesian updating on the force coefficients using the MCMC algorithm explained in Sec. 4. An uncertainty of 1 N standard deviation was assumed in the (measured) mean force data. The prior marginal pdfs of the force coefficients were taken as uniform. Figure 10 shows the prior and posterior distributions of the force coefficients. The force coefficient values obtained by the linear regression approach are identified by the "x"symbols. Note that the histograms were normalized to obtain a unit area

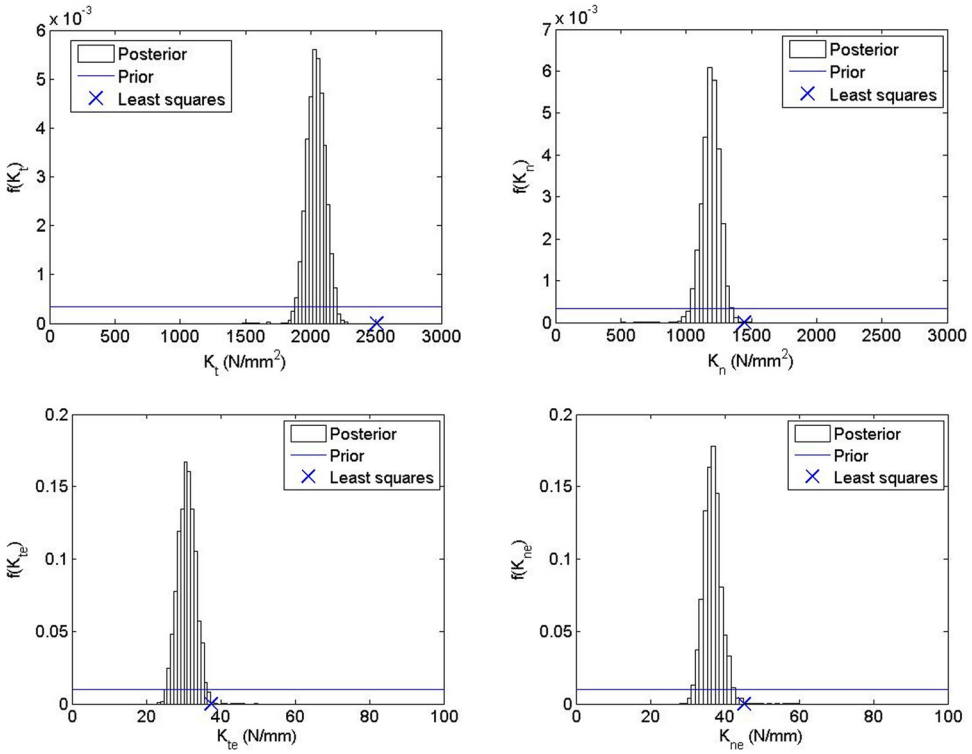

Fig. 13 Posterior and prior distributions of K_t (top left), K_n (top right), K_{te} (bottom left), and K_{ne} (bottom right)

Table 10 Correlation coefficients between the force coefficients at 50% radial immersion

	K_t	K_n	K_{te}	K_{ne}
K_t	1.00	0.08	−0.93	−0.28
K_n	0.08	1.00	0.13	−0.94
K_{te}	−0.93	0.13	1.00	0.06
K_{ne}	−0.28	−0.94	0.06	1.00

Table 11 Comparison of the posterior force coefficient distributions at 25% and 50% radial immersions

RI (%)	K_t (N/mm^2)	K_n (N/mm^2)	K_{ne} (N/mm)	K_{te} (N/mm)
25	N(2116.7, 137.3)	N(1284.4, 130.2)	N(35.5, 3.2)	N(37.4, 3.2)
50	N(2052.8, 67.8)	N(1187.8, 68.9)	N(30.4, 2,3)	N(36.7, 2.6)

under the curve. Figure 10 shows that the means of the posterior distributions for the force coefficients agree with the values obtained from the linear regression. Table 8 lists the correlation coefficients between the force coefficients obtained from the MCMC algorithm; they are similar to the values listed in Table 4. The experimental force profile at 0.05 mm/tooth was compared with the simulated force profile calculated using the posterior mean values of the force coefficients obtained from MCMC and the least squares values. Figure 11 shows the force profiles for F_x (left) and F_y (right). It is observed that the force coefficients from both methods approximate the experimental force profile well.

A second test was completed at 50% RI with all other parameters the same. Figure 12 shows the linear least squares fit to the experimental mean forces in the x and y directions. The mean force in x direction does not show a clear linear trend (because it is approximately zero for a 50% RI and near the noise limit) and, therefore, the quality of fit is not good ($R^2 = 0.70$). The least squares fit to the y direction mean forces is very good ($R^2 = 0.99$), however. As shown in Eqs. (8)–(11), the cutting force coefficients, K_t and K_n, and the edge coefficients, K_{te} and K_{ne}, are not

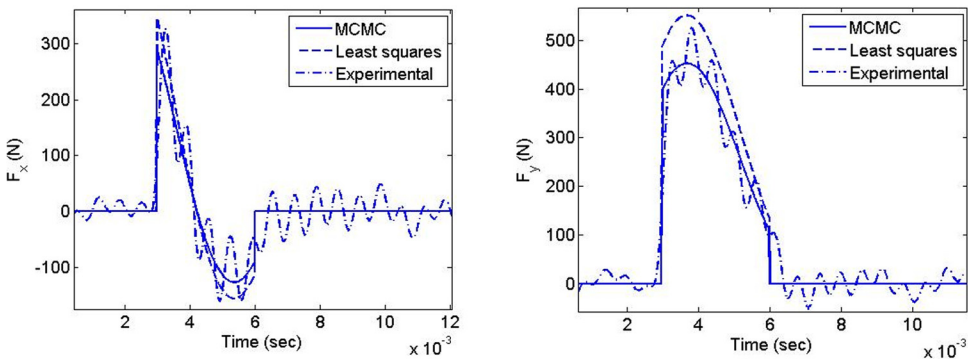

Fig. 14 Comparison of the experimental and simulated force profiles for F_x (left) and F_y (right)

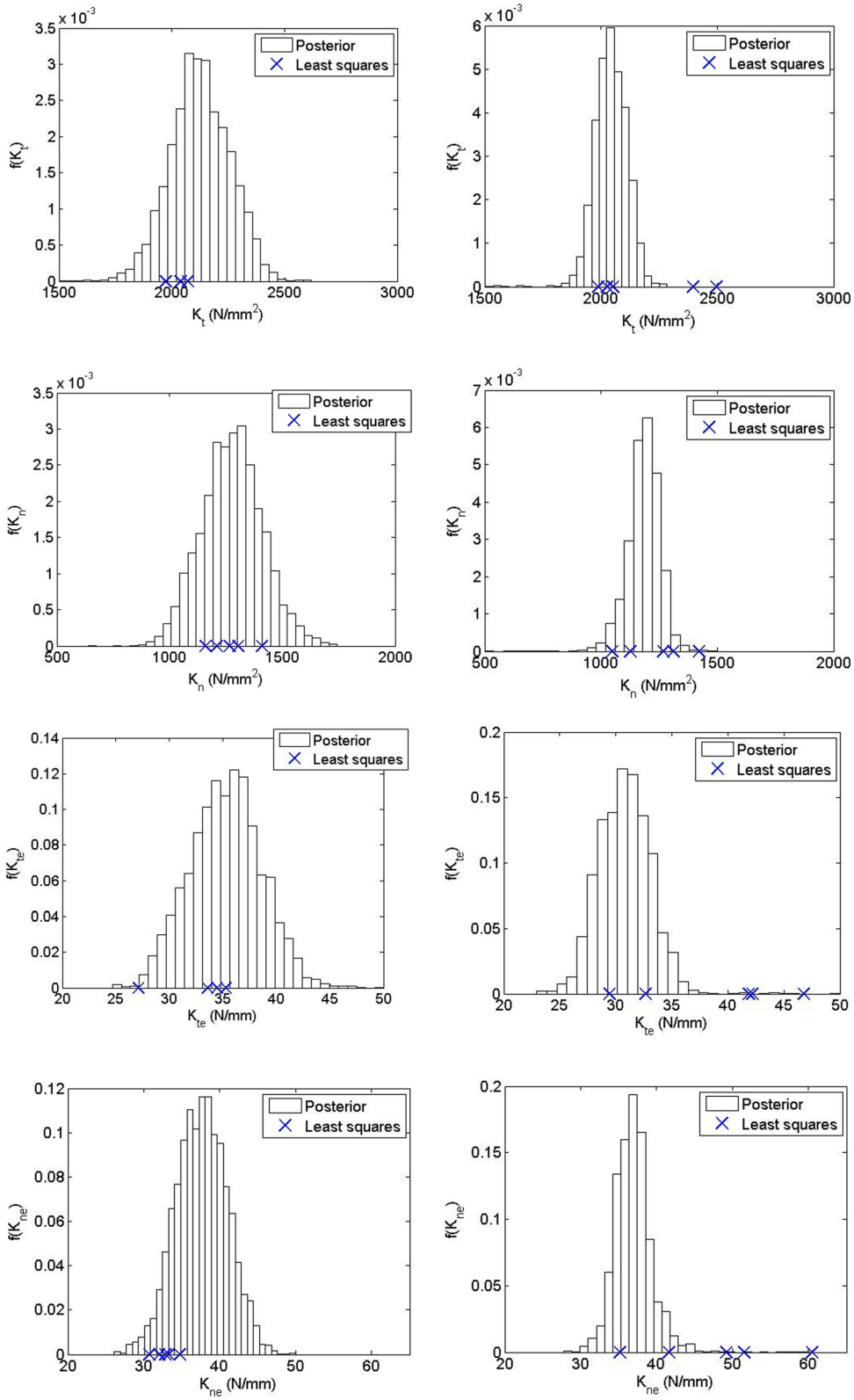

Fig. 15 Posterior distributions of force coefficients at 25% RI (left) and 50% RI (right)

decoupled, but depend on the slopes and intercepts of the least squares fits in both the *x* and *y* directions. Therefore, a poor fit in the *x* direction mean forces affects the values of all coefficients. Table 9 shows the mean forces in *x* and *y* directions and the force coefficients obtained using the linear regression approach.

The mean force data listed in Table 9 was used to update the force coefficients distribution by the MCMC algorithm. Figure 13 shows the prior and posterior distribution of the coefficients. Table 10 lists the correlation coefficients between the force coefficients from the MCMC analysis. As shown in Fig. 13, the force coefficient posterior distributions do not agree with the values obtained using the linear regression. This is due to poor least square fit for the mean *x* direction force. However, since the Bayesian updating does not rely on a curve fit, the posterior distributions are not

Table 12 Force coefficient values from the five tests at 25% RI

Test #	K_t (N/mm^2)	K_n (N/mm^2)	K_{te} (N/mm)	K_{ne} (N/mm)
Least squares results				
1	2149.0	1290.1	34.7	37.1
2	2071.2	1159.3	27.1	30.7
3	1973.9	1210.0	34.4	34.7
4	2055.0	1337.5	33.3	32.3
5	2173.0	1370.6	35.1	35.8
6	1972.6	1265.5	33.5	32.0
μ	**2065.8**	**1271.1**	**33.0**	**33.8**
σ	**84.5**	**78.6**	**3.0**	**2.5**
MCMC results				
	N(**2116.7**, **137.3**)	N(**1284.4**, **130.2**)	N(**35.5**, **3.2**)	N(**37.4**, **3.2**)

Table 13 Force coefficient values from the five tests at 50% RI

Test #	K_t (N/mm^2)	K_n (N/mm^2)	K_{te} (N/mm)	K_{ne} (N/mm)
Least squares results				
1	2504.6	1446.2	37.5	45.2
2	2496.4	1422.7	41.8	51.5
3	2396.6	1310.5	46.7	60.4
4	2025.7	1126.8	29.4	35.1
5	1987.8	1048.4	32.6	41.6
6	2052.5	1268.0	42.1	49.1
M	**2243.9**	**1270.4**	**38.3**	**47.1**
Σ	**246.93**	**158.51**	**6.47**	**8.70**
MCMC results				
	N(**2052.8**, **67.8**)	N(**1187.8**, **68.9**)	N(**30.4**, **2.3**)	N(**36.7**, **2.6**)

affected by the quality of the fit. Table 11 compares the force coefficient posterior distributions at 25% and 50% RI for the MCMC analysis. The force coefficients are insensitive to the radial immersion (as expected) for Bayesian updating and the posterior distributions obtained at 25% and 50% RI agree closely. Note that the variance of the posterior distribution for the 50% RI result is smaller than for the 25% RI result. The uncertainty in the mean force was assumed to be 1 N in both cases and both the x and y direction mean forces were used for updating. However, the mean y direction force magnitude at 50% RI is greater than 25%, which results in a lower signal to noise ratio for the 50% RI y direction forces and a smaller variance for the corresponding posterior distributions. Figure 14 shows the comparison between the experimental force profile at 0.05 mm/tooth and the simulated force profile using the posterior mean force coefficient values obtained from the MCMC and the least squares methods. It is seen that the peak force values in the x and y directions for the least squares force coefficient values is not in agreement with the experimental peak values, while the mean posterior force coefficient values agree with the experimental profile. This is because the force coefficient values obtained using the least squares method were higher than the values determined using the MCMC method.

6 Discussion

Bayesian updating using the MCMC Bayesian inference technique to determine force coefficients was presented. The advantage of using a Bayesian approach is that it takes into account both initial beliefs (prior knowledge) and experimental data to update beliefs. The Bayesian inference approach also takes into account the inherent uncertainty in force coefficients. As a result, force coefficients are characterized by a probability density function as opposed to a deterministic value. To validate the posterior force coefficient distributions, five additional tests were completed at radial immersions of 25% and 50%. Figure 15 shows the posterior distributions of the force coefficients at 25% (left) and 50% (right). The figure shows that the posterior distributions of force coefficients agree well with the least squares values at 25% RI. However, the force coefficient values obtained by linear regression at 50% RI do not agree with the posterior distributions. As shown in Fig. 12, this is due to a poor quality of least squares fit to the mean forces in the x direction.

Bayesian updating was performed using the mean force data from all the six tests (one experimental and five validation tests) at 25% and 50% RI. The values of the force coefficients obtained using the least squares method for the six tests at 25% and 50% RI are listed in Tables 12 and 13, respectively. The posterior mean and standard deviation value of the force coefficients at 25% and 50% using the MCMC approach are also listed. The mean and standard deviation calculated from the linear regression force coefficient values agree reasonably well with the posterior mean and standard deviation of the force coefficients. However, Bayesian inference reduces the need to perform experiments over multiple feed per tooth values, which can be time consuming and costly, by combining prior knowledge and experimental data. Therefore, the uncertainty in the force coefficients can be evaluated using a single or a few experimental results.

7 Conclusions

Bayesian updating of the force coefficients using the Markov chain Monte Carlo (MCMC) method was presented. The single component Metropolis Hastings (MH) algorithm of MCMC was used. Bayesian inference provides a formal way of belief updating when new experimental data is available. It gives a posterior distribution that incorporates the uncertainty in variables as compared to traditional methods, such as the linear regression which yields a deterministic value. By combining prior knowledge and experimental results, Bayesian inference reduces the number of experiments required for uncertainty quantification. Using Bayesian updating, a single test can provide distributions for force coefficients. The posterior distribution samples provide the covariance of the joint distribution as well. Experimental milling results showed that the linear regression did not give consistent results at 50% RI due to a poor quality of fit in the x direction mean forces, whereas Bayesian updating yielded consistent results at both radial immersions tested. Also, since Bayesian updating does not rely on a least squares fit, mean force data at different feed per tooth values is not required.

Finally, the Metropolis Hastings algorithm is a powerful tool for updating multiple variables. A grid-based method would require N^m computations, where m is the number of variables and N is the size of the grid. To illustrate, for a joint pdf of four variables with a grid size equal to 300, the grid-based method would require at least 8.1×10^9 computations. The MH algorithm would require only approximately 1×10^4 iterations for the value to converge to the posterior pdf mean values. The single component MH algorithm for MCMC facilitates updating of joint distributions without significant computational expensive.

References

[1] Schmitz, T., and Smith, K. S., 2009, *Machining Dynamics: Frequency Response to Improved Productivity*, Springer, New York.

[2] Kumanchik, L., and Schmitz, T., 2007, "Improved Analytical Chip Thickness Model for Milling," Precis. Eng., **31**, pp. 317–324.

[3] Andrieu, C., de Freitas, N., Doucet, A., and Jordan, M., 2003, "An Introduction to MCMC for Machine Learning," Mach. Learn., **50**, pp. 5–43.

[4] Metropolis, N., Rosenbluth, A. W., Rosenbluth, M. N., Teller, A. H., and Teller, E., 1953, "Equations of State Calculations by Fast Computing Machines," J. Chem. Phys., **21**(6), pp. 1087–1092.

[5] Hastings, W. K., 1970, "Monte Carlo Sampling Methods Using Markov Chains and Their Applications," Biometrika, **57**, pp. 97–109.

[6] Roberts, G. O., Gelman, A., and Gilks, W. R., 1997, "Weak Convergence and Optimal Scaling of Random Walk Metropolis Algorithms," Ann. Appl. Probab., **7**(1), pp. 110–112.

[7] Chib, S., and Greenberg, E., 1995, "Understanding the Metropolis Hastings Algorithm," The Am. Stat., **49**(4), pp. 327–335.

[8] Gelfand, A., and Smith, A., 1990, "Sampling-Based Approaches to Calculating Marginal Densities," J. Am. Stat. Assoc., **85**(410), pp. 398–409.

[9] Duncan, G. S., Kurdi, M., Schmitz, T., and Snyder, J., 2006, "Uncertainty Propagation for Selected Analytical Milling Stability Limit Analyses," Trans. NAMRI/SME, **34**, pp. 17–24. Available at: http://plaza.ufl.edu/mhkurdi/namrc.pdf